Nickel Complexes derived from Novel Phenylthiosemicarbazone ligands as Antimicrobial and Anticancer Agents: Synthesis, Characterization and Biological Investigations

Shivani B. Malap[1], Raju M. Patil[2]

[1,2] Department of Chemistry, The Institute of Science, Dr. Homi Bhabha State University, 15, Madam Cama Road, Mumbai – 400 032, (M.S.), India

***Abstract*—The present study deals with synthesis of series of novel Nickel(II) complexes derived from Isonitrosoacetophenone-4-Phenylthiosemicarbazones. The newly synthesized complexes have been fully characterized by spectroscopic and physiochemical methods like elemental analysis, UV-Visible, FTIR, 1H-NMR, Conductivity, TG-DTA, Cyclic Voltammetry and Magnetic Suceptibility Measurements. XRD analysis has also been used as an additional method to learn about crystal symmetry. All the complexes appear to be in crystalline phases based on the XRD pattern. To study the electrochemical behaviour of Nickel(II) complex Cyclic voltammetry was used. This showed that the ligand peaks changed significantly and new peaks appeared after the complexation process. The complexes have also been studied for their biological activity against four selected bacterial strains for antibacterial activity and two fungal strains for its antifungal activity. According to antimicrobial investigation both antibacterial and antifungal activity of complexes was higher than those of the ligands.The Complexes have also been tested for its Anti cancer activity against MDA-MB-231 Breast cancer cell line.**

***Index Terms*—Isonitrosoacetophenones, 4-Phenylthiosemicarbazones, Polydentate ligands, Antimicrobial activity, Transition metal complexes.**

I. INTRODUCTION

In recent years, a variety of organic ligands and metal ions have been used to build coordination complexes and their biological activities have been satisfactorily assessed both in vitro and in vivo [1]. With thione-thiol tautomers in solution, thiosemicarbazones are a significant class of polydentate ligands that display a variety of coordination patterns [2]. Furthermore, metal thiosemicarbazones have gained increasing attention in recent years due to their variety of biological characteristics, particularly as antiviral, antibacterial, antifungal and anticancer agents [3]. It has been demonstrated that thiosemicarbazones with a thiol group block the enzyme ribonucleotide reductase, which is involved in DNA synthesis [3]. Therefore, it is possible to stop DNA replication and cell formation by suppressing or halting the activity of the ribonucleotide reductase enzyme [4].

Additionally, numerous thiosemicarbazone compounds have been documented, with a focus on their ability to bind and cleave DNA [5]. Thiosemicarbazones are hence cytotoxic. It's interesting to note that metal coordination with the ligand affects the complex's lipophilicity, indicating that metal recognition increases the compound's cytotoxicity. In order to explore the intricate molecular details of their various biological functions, a subsequent number of transition metal thiosemicarbazone complexes have been synthesized and structurally described [6].

We are constantly dealing with infectious diseases in the twenty-first century [7], which have a significant global death and morbidity rate. Among infectious diseases, malaria is one particular condition that contributes to the global state of poor health. Patients faced a terrible predicament due to the lack of a significant bacterial [8] medication. Since drug resistance is the most challenging public health issue, there is an urgent need for a low-toxic, economically cheaper priced drug with a positive biological response. Therefore, thiosemicarbazone ligands, which are important in biological chemistry and the pharmaceutical sectors, were synthesized in an effort to find an effective anti-infectious drug.

Additional research has been done on the complexation of thiosemicarbazone ligands with transition metals, particularly Co(II), Ni(II), Cu(II), and Zn(II) [9]. This is because these metals have a significant biological response to control the pathogen infection due to their hydrophobicity, structural diversification, lipophilicity, chelation, penetration power, good therapeutic index, and other qualities that are crucial for pharmaceutical drugs.

In many biological processes, these metal complexes are also employed as catalytic cycles for enzymes. Therefore, due to their important properties as antioxidant [10], anticancer [11,12], anti-inflammatory [13], antimalarial [14,15], antimicrobial [16], anti-tuberculosis [17], etc., the therapeutic applications of Co(II), Ni(II), Cu(II), and Zn(II) complexes of thiosemicarbazone ligands are the focus of investigation. Thus, the Co(II), Ni(II), Cu(II), and Zn(II) complexes based on thiosemicarbazone ligands are a renowned class of coordination molecules for drug development.

In continuation to our previous work [18] in this communication, we therefore illustrate the synthesis and structural characterization of a Ni(II) complexes obtained from isonitrosoacetophenones-phenylthiosemicarbazone ligands bearing (N-N-S) donor sites. Antimicrobial efficacy of ligands and the complexes both were evaluated on selected bacterial and fungal strains.

II. EXPERIMENTAL

2.1. Materials and Methods

All chemicals utilized were of analytical grade (AR) and exhibited the highest level of purity. $NiCl_2.6H_2O$ was sourced from SDFCL and utilized directly without purification. Solvents like ethanol whenever used were distilled and purified according to standard procedure [[19]]. 4-Phenylthiosemicarbazide and para modified isonitrosoacetophenones were used for synthesis of the ligands [18]. A Shimadzu UV-1800A spectrophotometer was used to record the UV-visible absorption spectrum in dimethylformamide at a concentration of 10^{-3} M. The INFRA-3000 spectrophotometer was used to record infrared spectra. The Bruker Advance 400 MHz model was used to record ^{1}H-NMR.The room temperature magnetic susceptibility measurements was carried on Guoy's Balance GMX-02 model. The TG-DTA analysis was carried on RIGAKU Thermoplus 8120 Instrument. The cyclic voltammetry studies was carried on SP-300 Instrument. The electrical conductance in DMF solution (10^{-3}M) was recorded on EQUIP-TRONICS conductivity instrument(EQ-660A) at room temperature.

2.2. Synthesis of Complexes:

The ligands were prepared by our reported method [18]. The preparation of nickel complexes was carried in 2:1 (L:M) molar ratio. The complexes derived from p-substituted isonitrosoacetophenones phenylthiolsemicarbazone were prepared by dissolving 2 moles of ligands in 20 ml ethanol and 1 mole of $NiCl_2.6H_2O$ metal salt in 10 ml ethanol; NH_3 was added dropwise with constant stirring. The pH was maintained between 7-8 and stirred for 30 minutes. The solid mass was separated by filtration and washed repeatedly with ethanol and dried safely (Yield – above 85%).

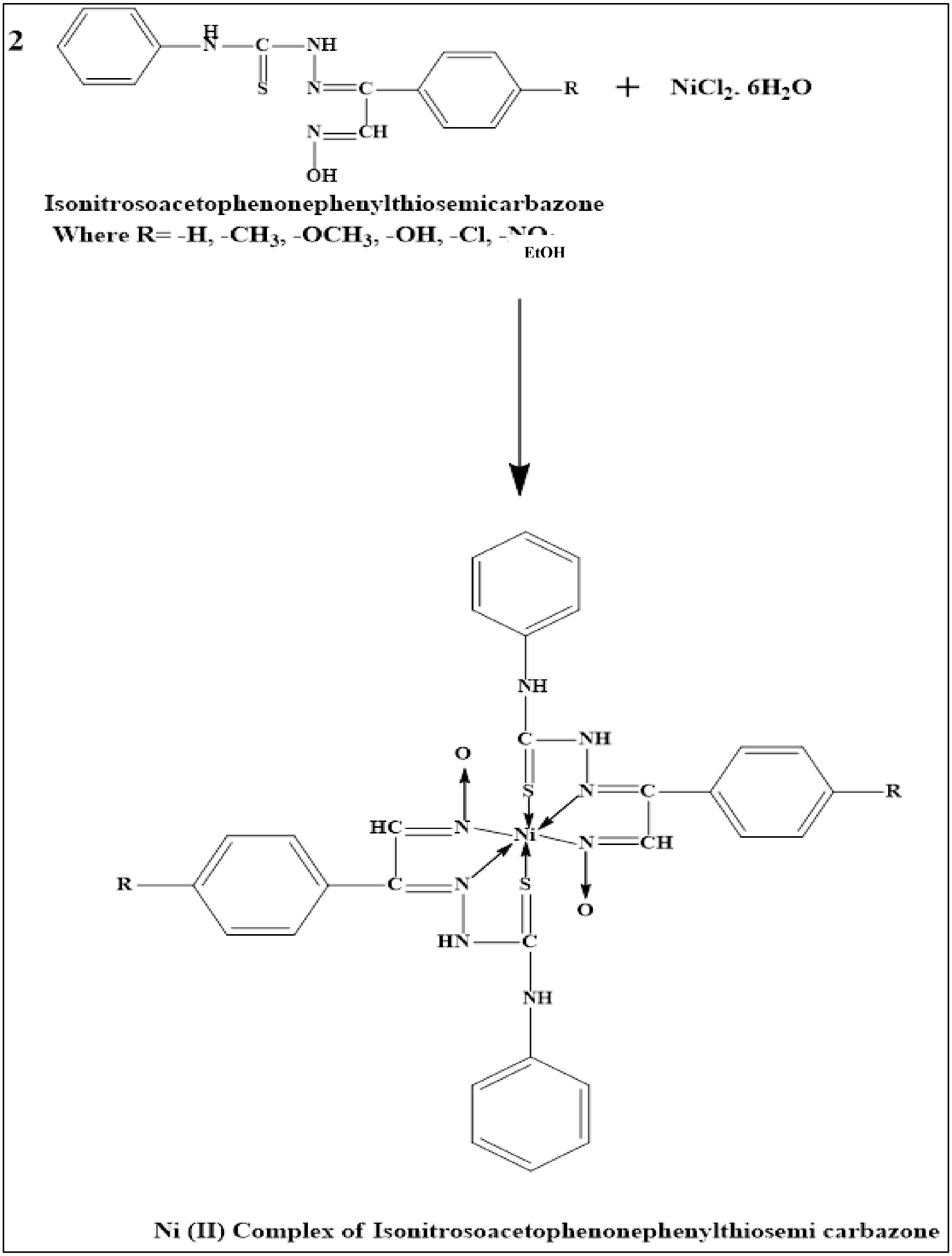

Scheme 1: General route for synthesis of Ni(II) complex of INAP-PTSC

2.3. Antimicrobial activities

The antibacterial and antifungal properties of the synthesized compounds were assessed using the well-cup diffusion technique. The study involved two fungal strains— *Saccharomyces cerevisiae* (MCC F1439)and *Candida albicans* (MCC F1033) and four bacterial strains— *Pseudomonas aeruginosa* (MCC 2080),*Escherichia coli* (MCC 2412),*Bacillus subtilis* (MCC 2010) and *Staphylococcus aureus* (MCC 2408). Ciprofloxacin and Fluconazole were employed as reference standards for antibacterial and antifungal activities, respectively.

Nutrient agar medium was sterilized by autoclaving at 121°C for 15 minutes and poured into sterile Petri dishes to solidify. The bacterial strains were freshly cultured in nutrient broth at 37°C for 18–24 hours to obtain active inocula. Similarly, Sabouraud Dextrose Agar (SDA) plates were prepared for fungal cultures, and the fungal strains were subcultured on SDA slants before use. Test compounds were dissolved in dimethyl sulfoxide (DMSO) to obtain 1 mg/mL solutions, and the standard drugs were prepared under identical conditions and concentrations for uniform comparison.

The criterion for microbial suspensions was 0.5 McFarland turbidity, which is roughly 10^8 CFU/mL for bacteria and 10^5 CFU/mL for fungi. Sterile cotton swabs were used to evenly distribute the solutions across the agar surface. Using a sterile borer, wells of 6 mm in diameter were aseptically made in the solidified agar. 50 µL of the test solution, standard, and control were then carefully poured into each well. Fungal plates were kept at 28°C for 48 hours, and bacterial plates were incubated at 37°C for 24 hours.

Following incubation, a ruler or digital caliper was used to measure the diameter of the inhibition zones surrounding each well in millimeters. Every assay was performed in triplicate, and the mean ± standard deviation was used to express the results. To verify that there was no intrinsic antibacterial activity, DMSO was used as the negative control and Ciprofloxacin and Fluconazole as the positive controls. The mean zone diameter from triplicate readings represented the final activity outcome after the observed inhibition zones of the synthesized compounds were compared with those of the standard medicines.

2.4. Anticancer Screening against MDA-MB-231 triple negative breast cancer cell lines using MTT assay:

MDA-MB-231 The triple negative breast cancer cell line, which was acquired from the National Cell Center in Pune, India, was used for the sample's MTT-based cytotoxicity test. A 96 well plate was seeded with 5000cells/100µL and incubated with 10% FBS (Fetal Bovine Serum) containing Dulbecco's Modified Eagle Medium(DMEM). After 48 hours, the 96-well plate was loaded with different concentrations of metal complexes during a 24-hour period. 10µL of 5mg/mL MTT reagent (dissolved in PBS) was applied to each well except the blank well and incubated at 37°C for 4 hours.After 4 hours, MTT solution was removed and 100µL of MTT solvent (4mM HCL in 100% isopropanol) was added to each well to dissolve the formazon crystals. Dissolution of formazon crystals was done by retro-pipetting gently and the plate was incubated at RT in dark for 5-10 mins. Absorbance was measured at 570nm using the BioTek Cytation. Cell Viability (%) was determined by following formula

$$\% \text{ Cell Viability} = [OD(\text{treated}) / OD(\text{control})] \times 100$$

III. RESULTS AND DISCUSSION

All of the complexes are solids that are stable and non-hygroscopic. They are brown in color and thermally stable. There is a satisfactory agreement between the elemental analysis results of the above synthesized complexes and the general formulation of the complexes. The complexes possess complete solubility in solvents like ethanol, DMF, CHCl3, and DMSO.

Table 1. Analytical and Physical Data of Complexes

Comp.	Subst	Molecular Formula	Molec Weight	% Elemental Analysis, Calculated (Observed)							μ_{eff} B.M.	Conductance mhos cm^2 mol^{-1}
				C	H	N	O	S	Cl	Ni		
NL1	-H	$C_{30}H_{26}N_8O_2S_2Ni$	653.3978	55.147 (55.145)	4.010 (4.007)	17.149 (17.142)	4.899 (4.918)	9.813 (9.809)	-	8.982 (8.979)	2.92	0.00089
NL2	-CH_3	$C_{32}H_{30}N_8O_2S_2Ni$	681.4524	56.401 (56.399)	4.437 (4.435)	16.443 (16.440)	4.698 (4.715)	9.409 (9.402)	-	8.612 (8.609)	2.85	0.00068
NL3	-OCH_3	$C_{32}H_{30}N_8O_4S_2Ni$	713.4502	53.872 (53.870)	4.238 (4.236)	15.705 (15.702)	8.972 (8.984)	8.987 (8.985)	-	8.226 (8.223)	2.92	0.00030
NL4	-OH	$C_{30}H_{26}N_8O_4S_2Ni$	685.3966	52.572 (52.570)	3.823 (3.821)	16.348 (16.344)	9.340 (9.352)	9.355 (9.353)	-	8.562 (8.560)	2.85	0.00040
NL5	-Cl	$C_{30}H_{24}N_8O_2Cl_2S_2Ni$	722.289	49.887 (49.885)	3.349 (3.346)	15.513 (15.510)	4.433 (4.447)	8.877 (8.875)	9.816 (9.815)	8.125 (8.122)	2.89	0.00063
NL6	-NO_2	$C_{30}H_{24}N_{10}O_6S_2$	743.393	48.470 (48.468)	3.253 (3.250)	18.841 (18.839)	12.917 (12.928)	8.625 (8.623)	-	7.894 (7.892)	2.89	0.00097

3.1. Conductivity Measurements

The electrical conductance of the complexes in DMF solution (0.001 M) were recorded on EQUIP-TRONICS conductivity instrument (EQ-660A) at room temperature using a conductivity cell and Pt as inert electrode. The complexes show molar conductance (3.08 - 9.72) x 10^{-4} mhos cm^2 mol^{-1} indicating non-electrolyte nature of complexes [20].

3.2. Magnetic Susceptibility measurements.

The studies on magnetic susceptibility measurements were conducted at room temperature (300K) utilizing Guoy's method, incorporating diamagnetic corrections. The complexes exhibit paramagnetic characteristics, displaying a magnetic moment within the range of 2.85 – 2.92 B.M. [20], which corresponds to the presence of two unpaired electrons and supports distorted octahedral geometry.

3.3. Electronic Spectra

The electronic UV-Visible spectra (Table 2) of the metal complexes in DMF (10^{-3} M) was recorded on SCHIMADZU UV 1800A Spectrophotometer in the range of 180–1100 nm. The spectra of all complexes shows three bands in the region of 19,417-24,096 cm^{-1}, 18,348-18,691 cm^{-1} and 14,903-15,479 cm^{-1} which could be attributed to $^3A_2g \rightarrow {}^3T_1g(P)$, $^3A_2g \rightarrow {}^3T_2g(F)$ and $^3A_2g \rightarrow {}^3T_1g(F)$ respectively which is similar to that of the Ni(II) distorted octahedral complexes[21].

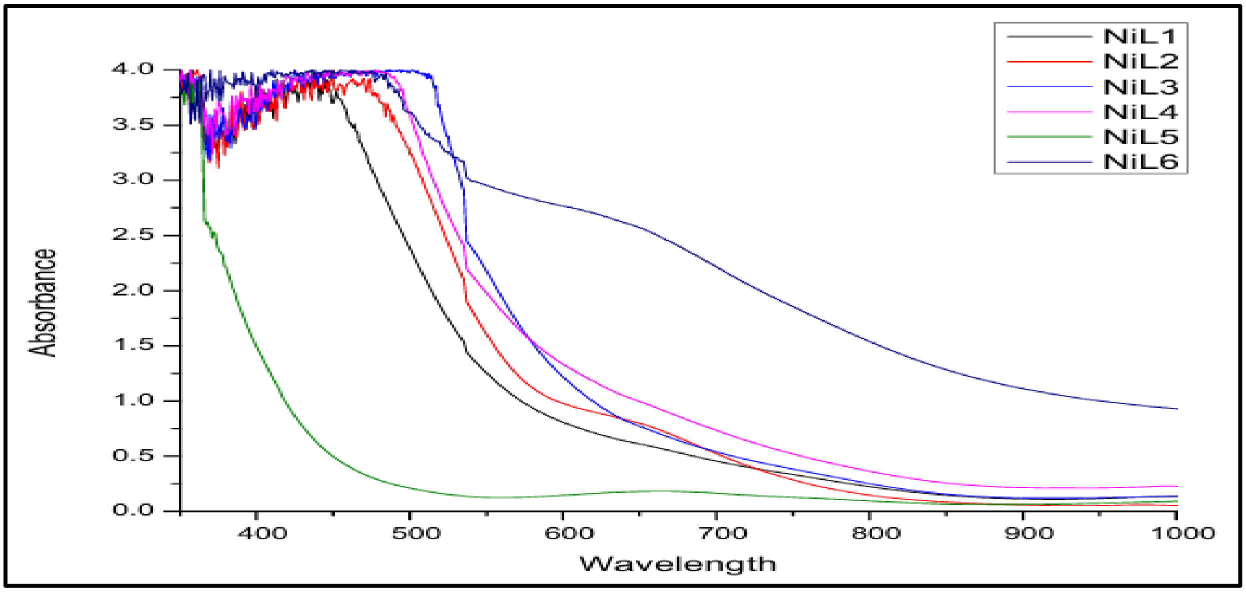

Fig.1. UV Visible Spectra of Complexes NL1–NL6

Table 2. Electronic Spectra of Complexes NL1 – NL6

Complex	(λ nm) υ cm^{-1}	Assignments	Complex	(λ nm) υ cm^{-1}	Assignments
NL1	(463) 21,598	$^3A_2g \rightarrow {}^3T_1g(P)$	NL4	(487) 20,533	$^3A_2g \rightarrow {}^3T_1g(P)$
	(535) 18,691	$^3A_2g \rightarrow {}^3T_2g(P)$		(535) 18,691	$^3A_2g \rightarrow {}^3T_2g(P)$
	(650) 15,384	$^3A_2g \rightarrow {}^3T_1g(F)$		(671) 14,903	$^3A_2g \rightarrow {}^3T_1g(F)$
NL2	(473) 21,141	$^3A_2g \rightarrow {}^3T_1g(P)$	NL5	(415) 24,096	$^3A_2g \rightarrow {}^3T_1g(P)$
	(536) 18,656	$^3A_2g \rightarrow {}^3T_2g(P)$		(536) 18,656	$^3A_2g \rightarrow {}^3T_2g(P)$
	(646) 15,479	$^3A_2g \rightarrow {}^3T_1g(F)$		(659) 15,174	$^3A_2g \rightarrow {}^3T_1g(F)$
NL3	(515) 19,417	$^3A_2g \rightarrow {}^3T_1g(P)$	NL6	(500) 20,000	$^3A_2g \rightarrow {}^3T_1g(P)$
	(545) 18,348	$^3A_2g \rightarrow {}^3T_2g(P)$		(535) 18,691	$^3A_2g \rightarrow {}^3T_2g(P)$
	(657) 15,220	$^3A_2g \rightarrow {}^3T_1g(F)$		(654) 15,290	$^3A_2g \rightarrow {}^3T_1g(F)$

3.4. FTIR Spectra

All of the complexes' FTIR spectra were recorded on INFRA-3000 in the range of 400–4000 cm^{-1}. The diagnostic IR spectrum of the representative complex NL1 (Fig.2.) was recorded, and the characteristic absorption bands of the complexes and their respective ligands are summarized in (Table 3**)**. The IR spectra of the free ligands displayed intense absorption peaks in the regions 1583–1600 cm^{-1} and 1662–1684 cm^{-1}, corresponding to ν(C=N)_oxime and ν(C=N)_imine stretching vibrations, respectively [18]. In the spectra of the nickel(II) complexes, these bands shifted to lower frequencies (1490–1550 cm^{-1} and 1573–1597 cm^{-1}), signifying the coordination of azomethine and oxime nitrogen atoms with the nickel ion [22]. The coordination was further confirmed by the appearance of new absorption bands in the ranges 470–495 cm^{-1} and 435–461 cm^{-1}, which are attributed to ν(N–Ni) and ν(N→Ni) vibrations, respectively, indicating the formation of a stable five-membered ring [23].

A broad band observed at 3026–3234 cm^{-1} in the free ligand spectrum, assigned to ν(O–H)_oxime, was absent in the spectra of the metal complexes, confirming deprotonation of the oxime hydrogen during coordination. The presence of the thioamide (–NH–C=S) group in the ligand allows for thione–thiol tautomerism [24]. However, the absence of a ν(S–H) stretching vibration (2500–2600 cm^{-1}) in the complexes indicates that the ligands retain their thione form in the solid state. The ν(C=S) band, observed in the range 836–920 cm^{-1} in the spectra of the free ligands, shifted to lower frequencies (747–830 cm^{-1}) upon complexation, suggesting participation of the thioketo sulfur in metal coordination [24]. This observation is further supported by the presence of ν(S→Ni) bands between 403–421 cm^{-1}.

Furthermore, sharp absorptions within 1020–1190 cm⁻¹, attributed to ν(N–O) in the ligands, shifted to 851–1009 cm⁻¹ in the complexes, representing ν(N→O) vibrations. Similarly, the ν(N–N) stretching band that appeared between 1230–1295 cm⁻¹ in the free ligands shifted slightly to 1213–1235 cm⁻¹ in the corresponding complexes, providing additional evidence for coordination through nitrogen atoms.

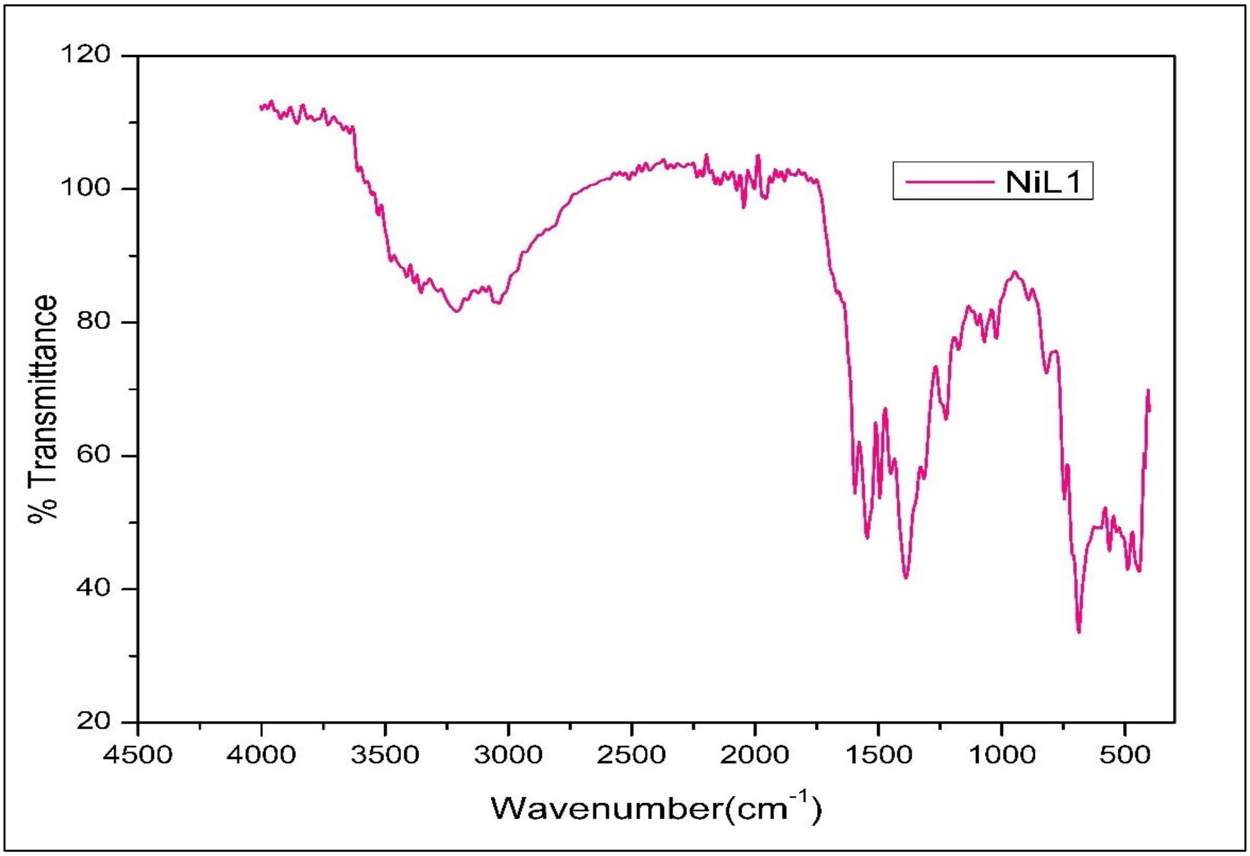

Fig.2. IR spectra of representative NL1 compound

Table 3. IR spectral data of Complexes (cm^{-1}).

Comp	ν(NH)	ν(C=N)$_{imine}$	ν(C=N)$_{oxime}$	ν(N-N)	ν(N→O)	ν(C=S)	ν(C-N)	Para Sub	ν(N-Ni)	ν(N→Ni)	ν(S→Ni)
NL1	3195	1595	1550	1221	903	808	730	-	485	435	413
NL2	3272	1597	1524	1221	895	747	715	675	470	445	413
NL3	3024	1595	1520	1215	940	815	720	672	473	447	413
NL4	3179	1597	1490	1235	951	830	748	684	495	445	403
NL5	3035	1573	1532	1213	854	813	755	675	495	461	403
NL6	3174	1597	1548	1229	1009	813	715	675	478	445	421

3.5. ^{1}H-NMR Spectra

The ^{1}H-NMR spectra of the synthesized Ni(II) complexes were recorded using a Bruker Avance 400 MHz spectrometer, and the spectral assignments for all complexes are summarized in **(**Table **4).** The spectrum of the representative complex NL2 (Fig.3.**)** displays distinct signals corresponding to amide and aromatic protons, while the characteristic proton signal of the =NOH group observed in the free ligand [18] is absent. This disappearance confirms complex formation through deprotonation of the oxime group and subsequent coordination of the nitrogen atom to the nickel center.

Notably, the methyl proton signals in the complexes appear at slightly lower chemical shift values compared to those in the corresponding ligand (L2). The aromatic proton resonances are observed at higher field regions between δ 6.811–7.660 ppm, indicating slight shielding effects upon complexation. The presence of the –NH– proton signal in the region δ 8.360–10.090 ppm, which is shifted upfield relative to that of the free ligands, provides further evidence for the thione form of the ligand in the complex.

Additionally, the =N–NH– proton appears at a higher chemical shift (δ 7.495–7.800 ppm) than in the ligand, while the –CH=N– proton exhibits a downfield shift, resonating at δ 3.148–3.334 ppm, suggesting coordination through the azomethine nitrogen. These spectral observations collectively confirm the proposed coordination mode of the ligands to the Ni(II) ion, and the results are consistent with those reported in earlier studies [25].

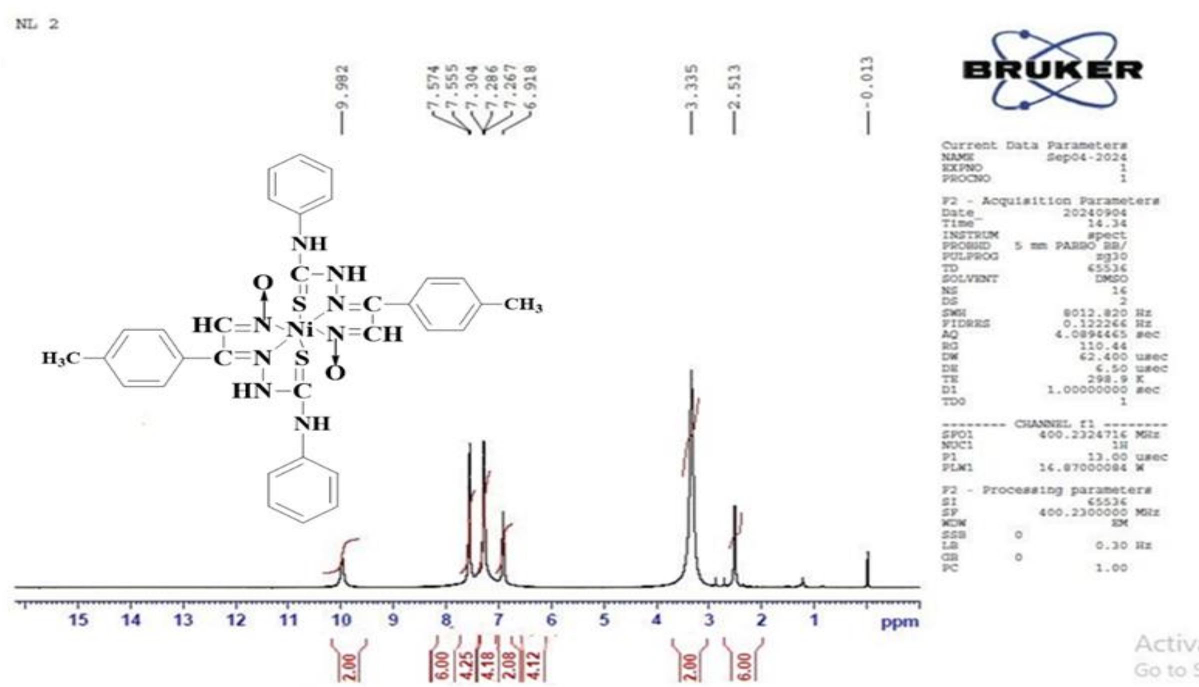

Fig.3. ^{1}H- NMR Spectra of representative compound NL2

Table 4. ^{1}H-NMR spectral data of complexes (δ in ppm).

Assignment	Chemical shift (δ in ppm)					
	NL1	NL2	NL3	NL4	NL5	NL6
-NH-	10.000	9.982	9.969	9.947	8.360	10.090
=N-NH-	7.800	7.574	7.800	7.776	7.567	7.495
-CH=N-	3.283	3.335	3.178	3.411	3.148	3.334
Ar-H	6.90-7.594	6.918 -7.555	6.903-7.554	6.811-7.535	6.889-7.260	6.863-7.202
-CH_3	-	2.513	-	-	-	-

$-OCH_3$	-	-	3.746	-	-	-
-OH	-	-	-	2.425	-	-

3.6. Thermal Analysis

A nitrogen atmosphere was used to conduct the simultaneous TG-DTA experiments of the synthesized complexes (Table 5**)** using the Rigaku Thermo Plus-8120 TG-DTA instruments. The temperature was increased from room temperature to 900°C at a rate of 10°C/min.

All the investigated complexes shows similar behavior in their thermogram. The complexes are stable upto 150^0C indicating absence of co-ordinated water molecule above that temperature there is continuous decomposition. The complex looses some moiety which could be attributed to partial loss of ligand INAP. The second step involves loss of some moiety which could be attributed to loss of PTSC. In the thermogram there is sudden decrease in weight suggests a simultaneous loss of ligands from the complex which is also reflected by strong endothermic peak in the DTA curve. Finally TG curve is stable above 600^0C where no loss in weight upto 900^0C indicating NiO as a final product of heating.

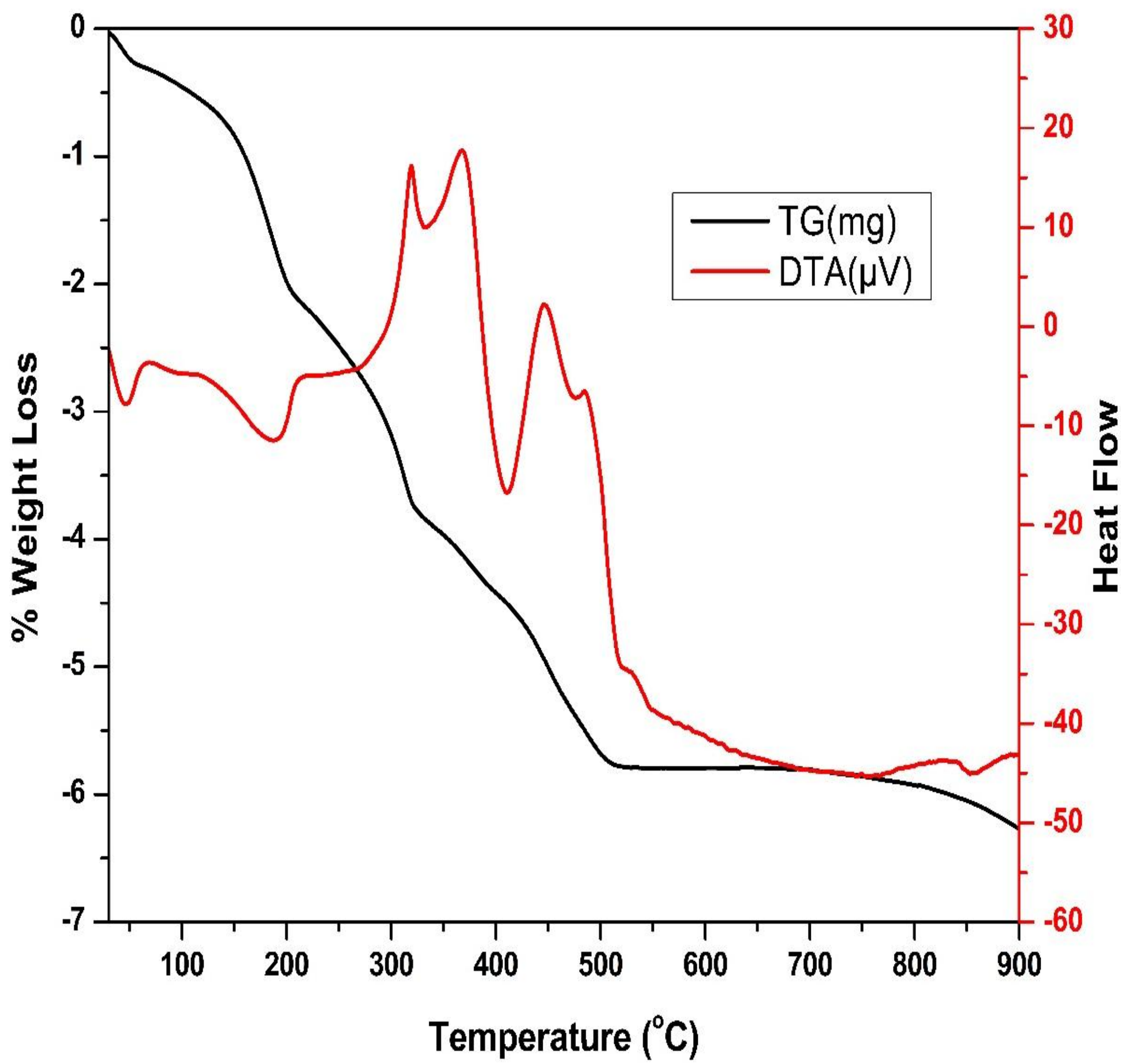

Fig.4. TG–DTA thermogram of representative compound NL1

Table 5. TG–DTA data of complexes

Complexes	% Loss Observed (Calculated)	Temperature (^{0}C)	Loss due to moiety
NL1	46.81 (46.88)	RT – 350	$C_{16}H_{14}N_6O$
	41.20 (41.15)	360-600	$C_{14}H_{12}N_2S_2$
	11.99(11.97)	>600	NiO
NL2	49.64 (49.58)	RT – 350	$C_{18}H_{18}N_6O$
	39.86 (39.80)	360-600	$C_{14}H_{12}N_2S_2$
	10.50 (10.62)	>600	NiO
NL3	51.39(51.35)	RT – 350	$C_{18}H_{18}N_6O_3$
	38.12(38.17)	360-600	$C_{14}H_{12}N_2S_2$
	10.49(10.48)	>600	NiO
NL4	49.49(49.44)	RT-350	$C_{16}H_{14}N_6O_3$
	39.68(39.74)	360-590	$C_{14}H_{12}N_2S_2$
	10.83(10.82)	>600	NiO
NL5	41.98(42.05)	RT – 350	$C_{16}H_{12}N_6O$
	47.77(47.72)	360-600	$C_{14}H_{12}N_2S_2Cl_2$
	10.25(10.23)	>600	NiO
NL6	53.14(53.10)	RT – 350	$C_{16}H_{12}N_8O_5$
	36.88 (36.85)	360-600	$C_{14}H_{12}N_2S_2$
	9.98 (10.05)	>600	NiO

3.7. Cyclic Voltammetry

The electrochemical characteristics of the synthesized Ni(II) complexes were investigated by cyclic voltammetry (Fig. 5.) using a three-electrode system consisting of a glassy carbon working electrode, a platinum counter electrode, and a saturated calomel electrode (SCE) as the reference. The measurements were carried out in 10^{-3} M DMF solution containing 0.1 M KCl as the supporting electrolyte, and the corresponding electrochemical data are summarized in **(**Table 6**)**.

All the mononuclear Ni(II) complexes, particularly NL3 and NL5, exhibited one irreversible oxidation peak on the anodic side and two irreversible reduction peaks on the cathodic side of SCE [26]. The cathodic waves observed at Epa values ranging from –0.038 to –0.552 V and –0.658 to –0.665 V were assigned to the Ni(II)/Ni(I) redox process and the ligand-centered reduction, respectively. On the anodic side, an irreversible oxidation response appeared within the potential range 0.581–1.169 V, corresponding to the Ni(II)/Ni(III) oxidation.

Further electrochemical studies in the potential range of 1.096–1.251 V vs SCE revealed three successive irreversible one-electron reduction processes in complexes NL1 and NL2, attributed to ligand-centered redox transitions involving Ni(II) ⇌ Ni(III), Ni(I) ⇌ Ni(II), and Ni(II) ⇌ Ni(I) couples. The redox potentials were found to be significantly influenced by the electronic nature of the substituent (R) on the phenyl ring of the 4-R-isonitrosoacetophenone ligands. Complexes containing electron-donating groups (e.g., R = OMe in NL3) displayed higher oxidation and reduction potentials, while those with electron-withdrawing substituents (e.g., R = Cl in NL5) exhibited lower values. These observations confirm that the substituent's electronic properties modulate the metal center's redox activity, and the appearance of new redox signals upon complexation further supports successful metal–ligand coordination [27–29].

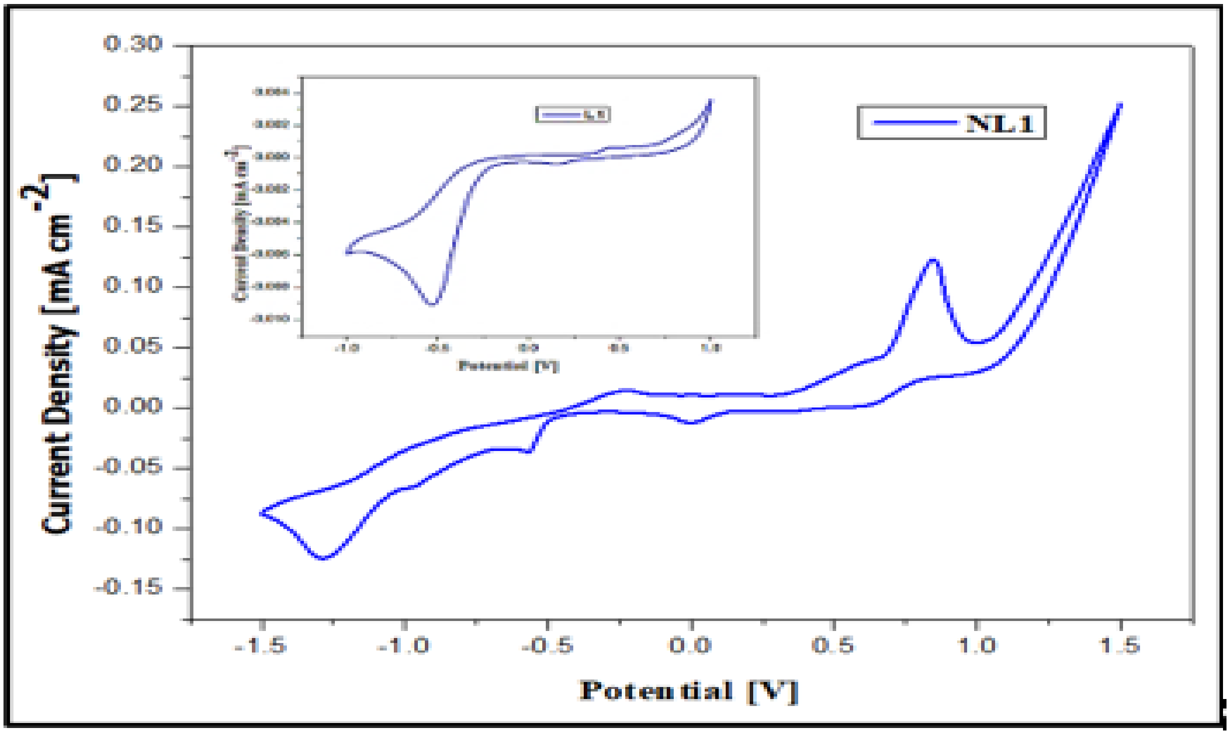

Fig. 5. Cyclic Voltagram of representative compound NL1

Table 6. Cyclic voltammetric data for Ni(II) complexes

Compound	Epc (V)	Epa (V)	ΔE= ǀEpa -Epcǀ (mV)	E^0 = (Epa -Epc)/2 (mV)
NL1	0.841	-0.012 -0.577	853	426.5
NL2	0.692	-0.033 -0.637	725	362.5
NL3	1.169	-0.552 -0.658	1721	860.5
NL4	1.066	-0.069 -0.692	1135	567.5
NL5	0.581	-0.038 -0.665	619	309.5
NL6	0.851	-0.520 -0.930	1371	685.5

3.8. Powder XRD

At 25^0C, with a bond angle (2θ) of $5\text{-}80^0$, the powder XRD of a subset of all complexes was recorded. The powder X-ray diffraction (XRD) patterns of complexes show crystalline nature with distinct differences in structural ordering. The particle size of crystalline compounds were also determined using powder XRD analysis.

The present Ni(II) complex showed a number of distinct and strong peaks in the XRD data (Table 7), with 2θ values are in the range $5.68\text{-}77.50^0$. The PXRD study verified that the complexes are semi-crystalline. Using the maximum intensity of the acquired line as a starting point, the Scherer equation was used to calculate the size of the crystalline particles.

$D = \frac{0.9\lambda}{\beta \cos\theta}$	Here, λ =X-ray wavelength(0.154nm), θ = Bragg diffraction angle, β = full width at half maximum (FWHM)

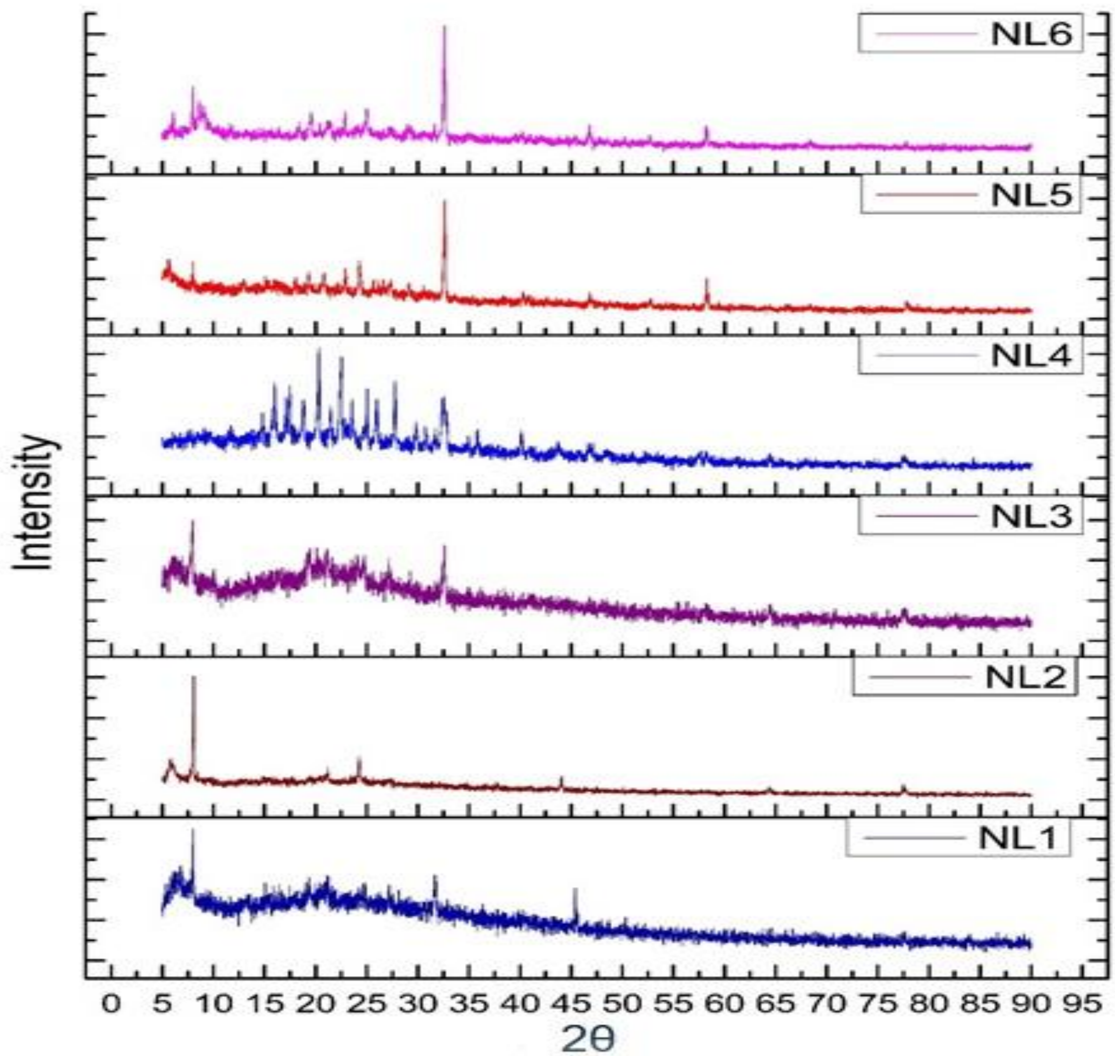

Fig.6. XRD Patterns of NL1-NL6 Complexes

Table 7. XRD data of Complexes NL1-NL6

Comp	2 θ (deg)	d (A)	FWHM (deg)	I	Avg. Particle Size(nm)	Comp	2 θ (deg)	d (A)	FWHM (deg)	I	Avg. Particle Size(nm)
NL1	8.28	10.667	0.300	11	31	NL4	11.66	7.583	0.280	18	71
	19.37	4.578	0.233	23			20.32	4.375	0.207	143	
	31.65	2.824	0.230	35			35.78	2.507	0.181	40	
	45.40	1.995	0.157	43			64.41	1.445	0.181	18	
	50.27	1.813	0.180	7			77.47	1.230	0.193	23	

NL2	8.03	10.989	0.107	350	33	NL5	5.68	15.546	0.190	37	87
	21.16	4.195	0.102	463			24.26	3.666	0.241	69	
	32.65	2.739	0.062	68			32.58	2.745	0.189	244	
	64.34	1.446	0.166	267			58.23	1.583	0.162	73	
	77.45	1.231	0.193	472			24.25	3.666	0.241	69	
NL3	7.91	11.168	0.340	57	41	NL6	7.97	11.079	0.144	79	89
	19.33	4.588	0.400	30			19.56	4.534	0.160	56	
	32.51	2.751	0.316	47			32.55	2.748	0.167	307	
	65.44	1.425	0.080	5			46.75	1.941	0.190	45	
	77.50	1.230	0.280	17			58.18	1.584	0.150	56	

3.9. Molecular Modeling study

The optimized structures of the Ni(II) complexes are shown in (Fig.7.), with bond lengths and angles summarized in **(**Table 8**)**. MM2 calculations using Chem3D Ultra indicate that the complexes adopt a distorted octahedral geometry around the nickel center. Spectroscopic data further support this proposed geometry.

Energy minimization results suggest that NL1 is the most stable complex, with a minimum energy of 256.3 kcal/mol. Differences in metal–nitrogen and metal–sulfur bond lengths confirm effective coordination of the ligand donor atoms to the metal ion. These computational findings align with the experimental spectral analyses, validating the proposed three-dimensional configuration and coordination mode of the synthesized Ni(II) complexes.

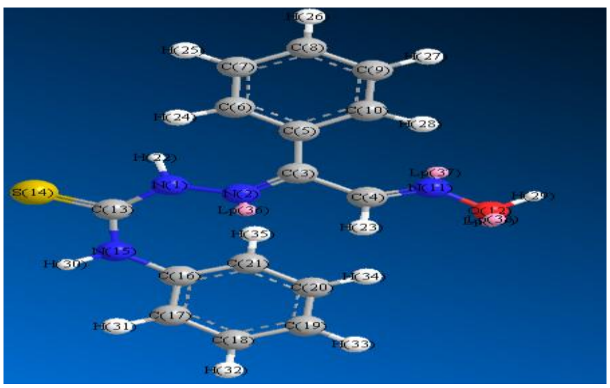

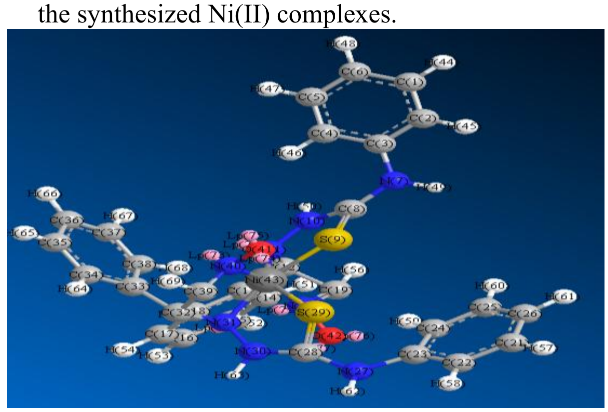

Fig.7. Optimised Structure of Ligand L1 and Complex NL1

Table 8. Bond angles and Bond lengths of Optimised Structure

Complex	Bonded atoms	Bond Length	Bonded atoms	Bond angle
NL1	C=S	1.6	N(20)-Ni(43)-N(40)	163.9660
	C=N	1.3	N(20)-Ni(43)-S(29)	86.6820
	N(20)-Ni(43)	1.8556	N(20)-Ni(43)-S(9)	99.6263
	N(40)-Ni(43)	1.8547	N(20)-Ni(43)-N(11)	74.5436
	S(29)-Ni(43)	2.1559	N(20)-Ni(43)-N(31)	83.1434
	S(9)-Ni(43)	2.1635	N(40)-Ni(43)-S(29)	80.8349
	N(11)-Ni(43)	1.8813	N(40)-Ni(43)-S(9)	90.0728
	N(31)-Ni(43)	1.8905	N(40)-Ni(43)-N(11)	121.1320
	N(20)-O(42)	1.3252	N(40)-Ni(43)-N(31)	83.0723
	N(40)-O(41)	1.3256	S(29)-Ni(43)-S(9)	88.2929

			S(29)-Ni(43)-N(11)	147.1020
			S(29)-Ni(43)-N(31)	69.4452
			S(9)-Ni(43)-N(11)	69.0820
			S(9)-Ni(43)-N(31)	157.4500
			N(11)-Ni(43)-N(31)	132.4570

3.10. Antimicrobial activity

The synthesized Ni(II) complexes were evaluated for their antimicrobial activity against four bacterial strains—two Gram-positive (*Bacillus subtilis* MCC 2010, *Staphylococcus aureus* MCC 2921) and two Gram-negative (*Escherichia coli* MCC 2412, *Pseudomonas aeruginosa* MCC 2080)—as well as two fungal strains, *Candida albicans* (MCC F1033)

Table *9*). Among the complexes, NL4 exhibited the highest activity against *B. subtilis* (–OH) group enhances activity through its electron-donating resonance effect and its ability to participate in hydrogen bonding with biological targets, thereby increasing binding affinity and disrupting cellular processes., while NL5 showed weak activity against *B. subtilis* and *S. cerevisiae* and was inactive against *S. aureus*, *P. aeruginosa*, *E. coli*, and *C. albicans* chloro (–Cl) substituent shows reduced activity. Although chlorine increases lipophilicity, its electron-withdrawing inductive (–I) effect decreases electron density on the coordinating azomethine nitrogen, weakening metal–ligand bonding and reducing biological effectiveness. Complex NL6 demonstrated excellent antibacterial activity against *P. aeruginosa* and *E. coli* (inhibition zones 18–22 mm) and equipotent activity against *B. subtilis* and *S. aureus*

and *Saccharomyces cerevisiae* (MCC F1439). Ciprofloxacin and Fluconazole were used as positive controls for antibacterial and antifungal assays, respectively, at the same concentrations.

The antimicrobial efficacy of the complexes, determined using the well-disc diffusion method, is represented in (Fig. *8*) and (

(13–14 mm), surpassing Ciprofloxacin (12 and 10 mm) The strong electron-withdrawing nature of the (–NO_2) group significantly alters the electronic distribution within the ligand, enhancing redox behavior and facilitating interactions with microbial enzymes. This substituent may also promote oxidative stress within microbial cells, contributing to the observed high activity..

Minimal inhibitory concentration (MIC) studies (Table 10) indicated that NL2 and NL4 exhibited superior bacteriostatic and fungistatic properties compared to other complexes and the positive controls. The enhanced activity of the metal complexes relative to the free ligands (Fig.9) can be attributed to chelation[30–32], which reduces the polarity of the metal ion through orbital overlap and partial charge sharing with the ligand. Additionally, the azomethine group may form hydrogen bonds with cellular targets, disrupting normal cell processes[33].

Table 9. Antimicrobial activity of NL1 – NL6

Comp.	Zone of Inhibition (mm)					
	Antibacterial Activity				Antifungal Activity	
	S. aureus	*B. subtilis*	*E. coli*	*P. aeruginosa*	*C. albicans*	*S. cerevsiae*
NL1	13	21	0	13	9	13
NL2	15	20	8	7	8	14
NL3	18	14	0	8	10	15
NL4	19	8	11	0	26	16
NL5	10	0	0	0	0	16
NL6	13	14	18	22	12	13

STD	12	10	13	18	17	18

Table 10. MIC Values of Antimicrobial activity of NL1 – NL6

Comp	Antibacterial Activity				Antifungal Activity	
	S. aureus	*B. subtilis*	*E. coli*	*P. aeruginosa*	*C. albicans*	*S. cerevsiae*
NL1	23.1	14.3	-	23.1	33.3	23.1
NL2	20	15	37.5	42.9	37.5	21.4
NL3	16.7	21.4	-	37.5	30	20
NL4	15.8	37.5	27.3	-	11.5	18.8
NL5	30	-	-	-	-	18.8
NL6	23.1	21.4	16.7	13.6	25	23.1
STD	25	30	23.1	16.7	17.6	16.7

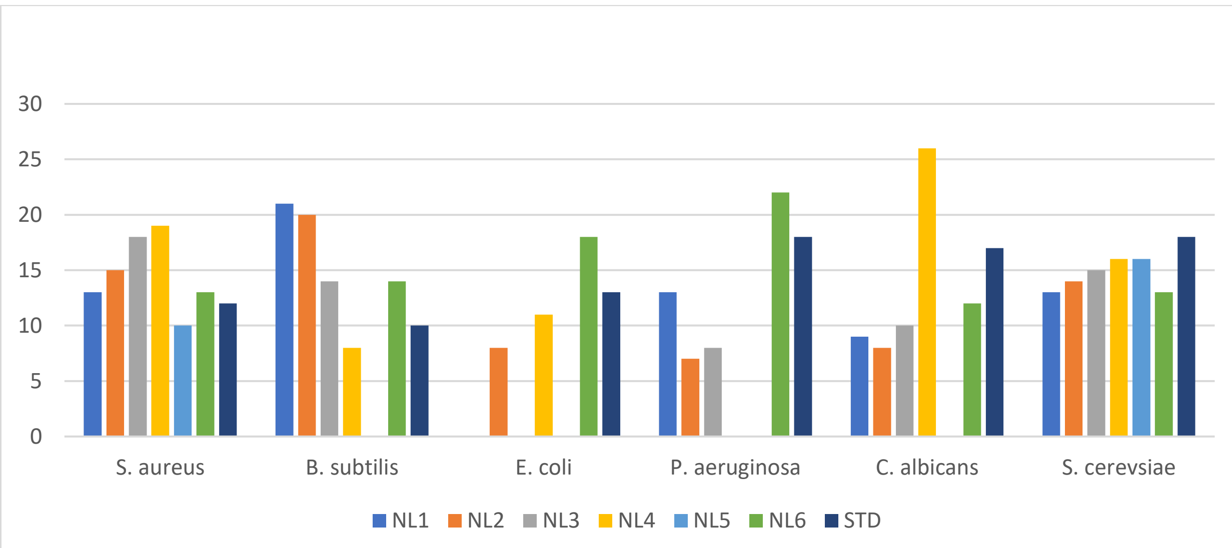

Fig. 8. Antimicrobial activity of Complexes NL1 – NL6

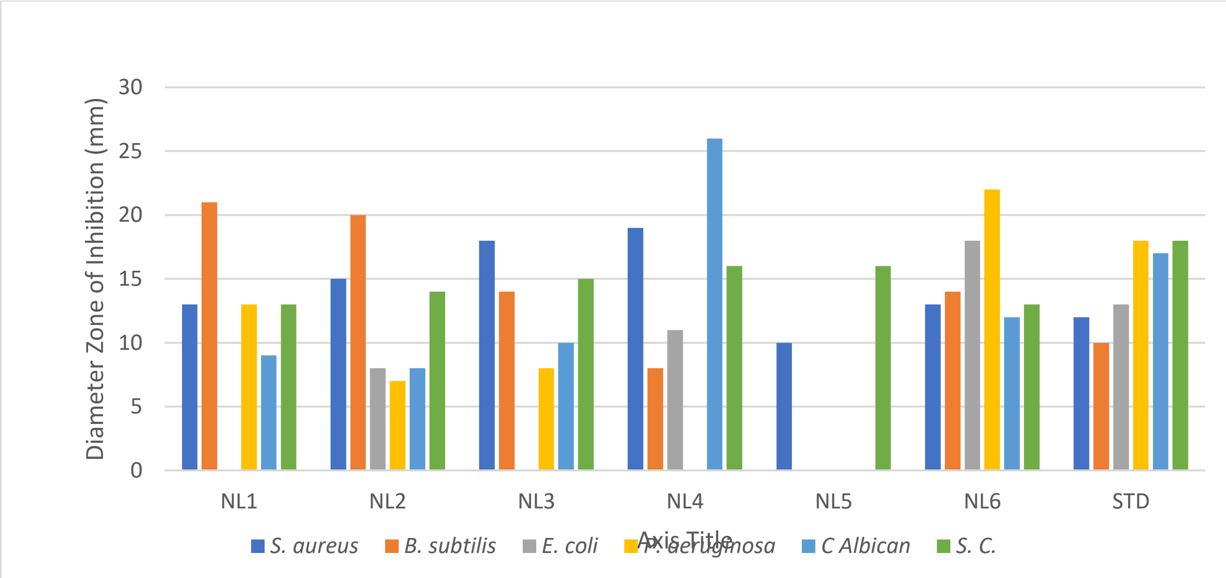

Fig.9. MIC of Antimicrobial activity of Complexes NL1 – NL6

3.11. Anticancer screening

Anti-cancer investigations of the compounds revealed substantial effectiveness against MDA-MB-231 cancer cells. The MDA-MB-231 cell line's average % cell viability and cytotoxicity statistics are displayed in

Table 11. The mean percent cell viability was used to calculate anticancer activity. Complex NL1 demonstrated a limited cytotoxic potential at all concentrations when compared to the conventional medications used in the study. When compared to the studied medications and the conventional Paclitaxel, the complex NL2 and NL3 showed only slight action when compared to free ligands.*(18)*. Both NL4 and NL6 showed activity, although NL5 was more effective against MDA-MB-231. The morphograph of NL5 (Fig.10). shows that the control cells are in good condition, as seen by their uniform cell surface and smooth appearance. Apoptotic features like membrane blebbing, cytoplasmic vacuolization, cell shrinkage, and small nuclei were observed in cells treated with NL5 at dosages ranging from 0.1 to 1000 (µg/ml). The MTT assay corroborated these findings.

According to the MTT data, test compound NL1 did not display any cytotoxicity across the range; test compounds NL2 and NL3 had marginal cytotoxicity, while NL4, NL5, and NL6 only shown considerable cytotoxicity on MDA-MB-231 cells at the highest concentration of 1000 µg/mL.The enhanced activity of the metal complexes relative to the free ligands can be attributed to chelation[30–32], which reduces the polarity of the metal ion through orbital overlap and partial charge sharing with the ligand. Additionally, the azomethine group may form hydrogen bonds with cellular targets, disrupting normal cell processes[33]

Table 11. Average values for % cell viability for the cell line MDA-MB-231

Concentration (µg/ml)	Average % Cell Viability					
	NL1	NL2	NL3	NL4	NL5	NL6
0	100	100	100	100	100	100
0.1	89.521	90.619	93.652	90.412	90.653	90.173
1	86.483	85.266	86.743	79.105	78.288	79.702
10	78.770	79.680	78.755	75.411	75.616	76.014
100	75.248	74.688	75.352	73.300	72.785	72.081
1000	70.145	71.082	71.628	62.500	63.228	59.006
PTX (10nM)	57.504	57.504	57.504	57.504	57.504	57.504

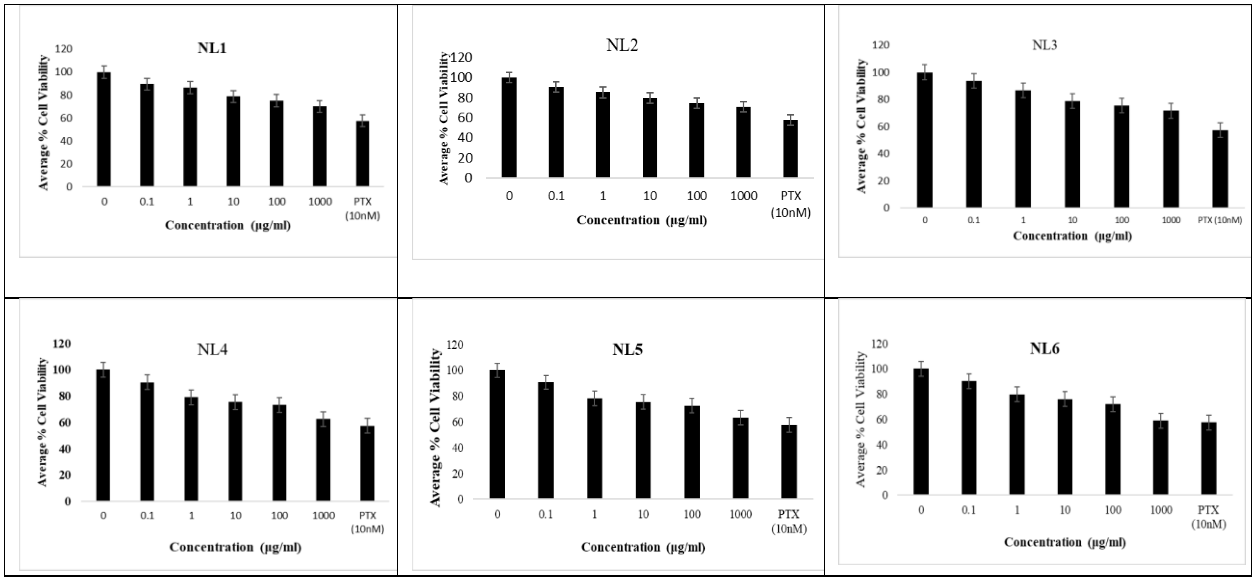

Fig.10. % Cell Viability against Concentration of complexes NL1 – NL6

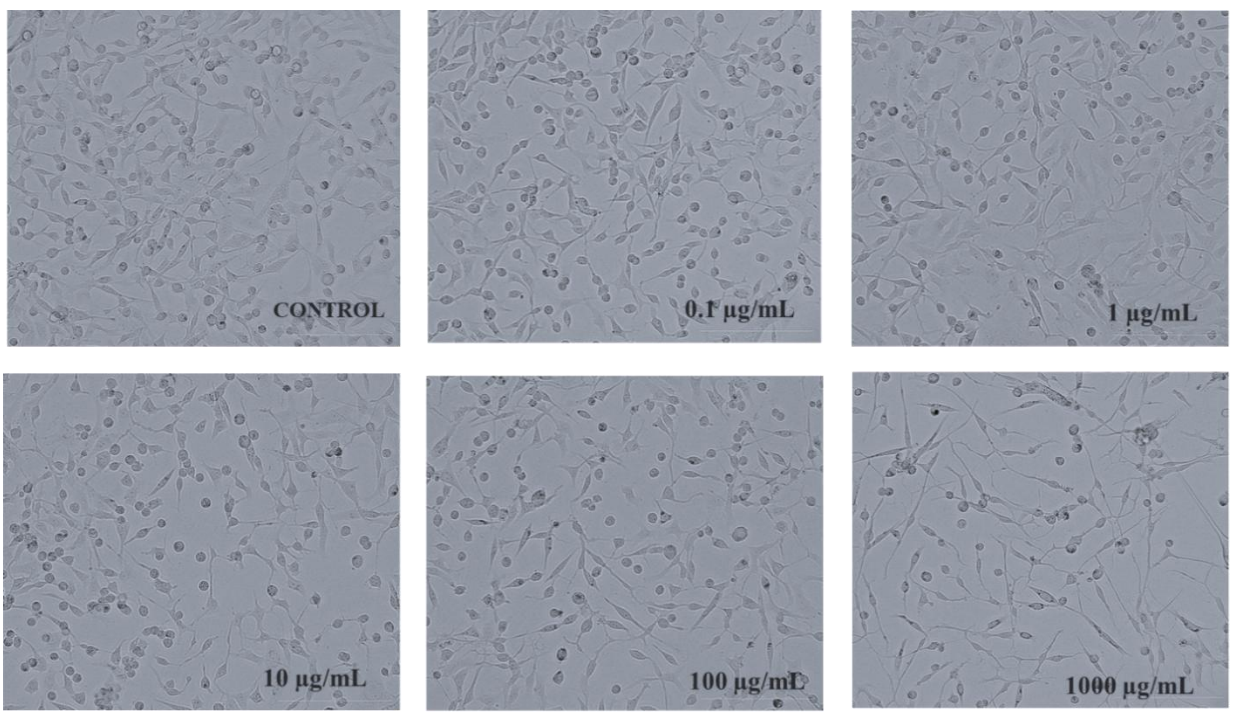

Fig.11. Morphological investigation of MDA-MB-231 cancer cells treated with Compound NL5 and control

IV. CONCLUSION

The Present Study successfully reports the synthesis and characterization of series of Novel Nickel(II) complexes derived of Isonitrosoacetophenonesphenylthiosemicarbazone (INAP-PTSC) ligands. Comprehensive spectroscopic and physiochemical analysis including UV-Visible, FTIR, ^{1}H-NMR, magnetic susceptibility and thermal studies confirmed the formation, stability and structural features of the complexes. The results reveals that the coordination of Nickel(II) ions with the thiosemicarbazone ligands enhances the overall stability and modifies the electronic environment of the metal center. Furthermore, biological screening demonstrated significant antimicrobial activity of the synthesized complexes against selected bacterial and fungal strains, surpassing that of the free ligands in several cases. Anticancer screening of complexes revealed moderate to higher toxicity compares to that of ligand. This enhanced bio activity can be attributed to the chelation effect, which increases lipophilicity and facilitates cell membrane penetration. Overall the findings highlight the potential of Nickel(II) complexes of INAP-PTSC's as promising candidates for the development of new pharmaceutical agents.

V. ACKNOWLEDGEMENT

Authors are grateful to The Institute of Science and Dr. Homi Bhabha State University, Mumbai for providing Instrumental and Laboratory Facilities.

REFERENCES

[1] Frezza, M.; Hindo, S.; Chen, D.; Davenport, A.; Schmitt, S.; Tomco, D.; et al. Novel Metals and Metal Complexes as Platforms for Cancer Therapy. *Current Pharmaceutical Design* 2010, *16*(16), 1813–1825. doi:10.2174/138161210791209009.

[2] Lobana, T. S.; Sharma, R.; Bawa, G.; Khanna, S. Bonding and structure trends of thiosemicarbazone derivatives of metals—An overview. *Coordination Chemistry Reviews* 2009, *253*(7–8), 977–1055. doi: 10.1016/j.ccr.2008.07.004.

[3] Pahontu, E.; Julea, F.; Rosu, T.; Purcarea, V.; Chumakov, Y.; Petrenco, P.; et al. Antibacterial, antifungal and *in vitro* antileukaemia activity of metal complexes with thiosemicarbazones. *Journal of Cellular and Molecular Medicine* 2015, *19*(4), 865–878. doi:10.1111/jcmm.12508.

[4] Sartorelli, A. C.; Moore, E. C.; Zedeck, M. S.; Agrawal, K. C. Inhibition of ribonucleoside diphosphate reductase by 1-formylisoquinoline thiosemicarbazone and related compounds. *Biochemistry* 1970, *9*(23), 4492–4498. doi:10.1021/bi00825a005.

[5] Ingle, S. A.; Kate, A. N.; Kumbhar, A. A.; Khan, A. A.; Rao, S. S.; Gejji, S. P. Synthesis and biological evaluation of copperpyrenethiosemicarbazone. *RSC Advances* 2015, *5*(59), 47476–47487. doi:10.1039/C5RA00020C.

[6] Gupta, S.; Singh, N.; Khan, T.; Joshi, S. Thiosemicarbazone derivatives of transition metals as multi-target drugs: A review. *Results in Chemistry* 2022, *4*, 100459. doi: 10.1016/j.rechem.2022.100459.

[7] Laryea, M. K.; Sheringham Borquaye, L. Antimalarial, Antioxidant, and Toxicological Evaluation of Extracts of Celtis africana, Grosseria vignei, Physalis micrantha, and Stachytarpheta angustifolia. *Biochemistry Research International* 2021, *2021*, 1–10. doi:10.1155/2021/9971857.

[8] Ajayi, A. M.; Coker, A. I.; Oyebanjo, O. T.; Adebanjo, I. M.; Ademowo, O. G. Ananas comosus (L) Merrill (pineapple) fruit peel extract demonstrates antimalarial, anti-nociceptive and anti-inflammatory activities in experimental models. *Journal of Ethnopharmacology* 2022, *282*, 114576. doi: 10.1016/j.jep.2021.114576.

[9] Damit, N. S. H. H.; Hamid, M. H. S. A.; Rahman, N. S. R. H. A.; Ilias, S. N. H. H.; Keasberry, N. A. Synthesis, structural characterisation and antibacterial activities of lead(II) and some transition metal complexes derived from quinoline-2-carboxaldehyde 4-methyl-3-thiosemicarbazone. *Inorganica Chimica Acta* 2021, *527*, 120557. doi: 10.1016/j.ica.2021.120557.

[10] Aly, S. A.; Hassan, S. S.; Eldourghamy, A. S.; Badr, E. E.; El-Salamoney, M. A.; Hassan, M. A.; et al. Synthesis, characterization, XRD, SEM, DNA binding, and effect of γ-irradiation of some new Ni (II) and Co (II) complexes with thiosemicarbazone ligand: In vitro antimicrobial and antioxidant activities. *Applied Organometallic Chemistry* 2022, *36*(9). doi:10.1002/aoc.6727.

[11] Devi, J.; Kumar, B.; Taxak, B. Recent advancements of organotin (IV) complexes derived from hydrazone and thiosemicarbazone ligands as potential anticancer agents. *Inorganic Chemistry Communications* 2022, *139*, 109208. doi: 10.1016/j.inoche.2022.109208.

[12] Carcelli, M.; Tegoni, M.; Bartoli, J.; Marzano, C.; Pelosi, G.; Salvalaio, M.; et al. In vitro and in vivo anticancer activity of tridentate

thiosemicarbazone copper complexes: Unravelling an unexplored pharmacological target. *European Journal of Medicinal Chemistry* 2020, *194*, 112266. doi: 10.1016/j.ejmech.2020.112266.

[13] Rani, M.; Devi, J.; Kumar, B. Thiosemicarbazones-based Co(II), Ni(II), Cu(II) and Zn(II) complexes: synthesis, structural elucidation, biological activities and molecular docking. *Chemical Papers* 2023, *77*(10), 6007–6027. doi:10.1007/s11696-023-02917-x.

[14] Mandal, A.; Kushwaha, R.; Mandal, A. A.; Bajpai, S.; Yadav, A. K.; Banerjee, S. Transition Metal Complexes as Antimalarial Agents: A Review. *ChemMedChem* 2023, *18*(19). doi:10.1002/cmdc.202300326.

[15] Aly, A. A.; Abdallah, E. M.; Ahmed, S. A.; Rabee, M. M.; Bräse, S. Transition Metal Complexes of Thiosemicarbazides, Thiocarbohydrazides, and Their Corresponding Carbazones with Cu(I), Cu(II), Co(II), Ni(II), Pd(II), and Ag(I)—A Review. *Molecules* 2023, *28*(4), 1808. doi:10.3390/molecules28041808.

[16] Gaber, A.; Refat, M. S.; Belal, A. A. M.; El-Deen, I. M.; Hassan, N.; Zakaria, R.; et al. New Mononuclear and Binuclear Cu(II), Co(II), Ni(II), and Zn(II) Thiosemicarbazone Complexes with Potential Biological Activity: Antimicrobial and Molecular Docking Study. *Molecules* 2021, *26*(8), 2288. doi:10.3390/molecules26082288.

[17] Kotian, A.; Kamat, V.; Naik, K.; Kokare, D. G.; Kumara, K.; Lokanath, N. K.; et al. Hydroxyacetone derived N4-methyl substituted thiosemicarbazone: Syntheses, crystal structures and spectroscopic characterization of later first-row transition metal complexes. *Journal of Molecular Structure* 2021, *1224*, 129055. doi: 10.1016/j.molstruc.2020.129055.

[18] Malap, S. B.; Patil, R. M. Synthesis, characterization and biological investigations of novel phenylthiosemicarbazones. *Journal of the Indian Chemical Society* 2025, *102*(9), 101933. doi: 10.1016/j.jics.2025.101933.

[19] Perrin, D. D. (Douglas D.; Armarego, W. L. F.; Perrin, D. R. *Purification of Laboratory Chemicals*; [1st ed.].; Pergamon Press, 1966.

[20] Mhadaye, M. E.; Patil, R. M. 63 | PARIPEX-INDIAN JOURNAL OF RESEARCH Synthesis and Characterisation of Nickel Metal Complexes Derived from Novel Hydrazone Derivatives. 2016.

[21] Sathisha, M. P.; Budagumpi, S.; Kulkarni, N. V.; Kurdekar, G. S.; Revankar, V. K.; Pai, K. S. R. Synthesis, structure, electrochemistry and spectral characterization of (d-glucopyranose)-4-phenylthiosemicarbazide metal complexes and their antitumor activity against Ehrlich Ascites Carcinoma in Swiss albino mice. *European Journal of Medicinal Chemistry* 2010, *45*(1), 106–113. doi: 10.1016/j.ejmech.2009.09.031.

[22] Nigam, S.; Patel, M. M.; Ray, A. Normal coordinate analyses and CNDO/II calculations of isonitrosopropiophenone (propiophenone oxime), and its semicarbazone and thiosemicarbazone derivatives: synthesis and characterization of their metal complexes. *Journal of Physics and Chemistry of Solids* 2000, *61*(9), 1389–1398. doi:10.1016/S0022-3697(00)00025-1.

[23] Chandra, S.; Vandana. Synthesis, spectroscopic, anticancer and antibacterial studies of Ni(II) and Cu (II) complexes with 2-carboxybenzaldehyde thiosemicarbazone. *Spectrochimica Acta - Part A: Molecular and Biomolecular Spectroscopy* 2014, *129*, 333–338. doi: 10.1016/j.saa.2014.02.141.

[24] Chandra, S.; Kumar, U. Spectral and magnetic studies on manganese (II), cobalt (II) and nickel (II) complexes with Schiff bases. *Spectrochimica Acta Part A: Molecular and Biomolecular Spectroscopy* 2005, *61*(1–2), 219–224. doi: 10.1016/j.saa.2004.03.036.

[25] Babahan, I.; Özmen, A.; Orhan, N.; Kazar, D.; Değirmenci, E. H. Synthesis, characterization, and in vitro anti-neoplastic activity of novel vic-dioximes bearing thiosemicarbazone side groups and their mononuclear complexes. *Bioorganic Chemistry* 2014, *53*, 92–98. doi: 10.1016/j.bioorg.2014.01.003.

[26] Choi, K.-Y.; Yang, S.-M.; Lee, K.-C.; Ryu, H.; Lee, C. H.; Seo, J.; et al. Synthesis, properties, and crystal structures of mononuclear nickel (II) and copper (II) complexes with 2-oximino-3-thiosemicarbazone-2,3-butanedione. *Transition Metal Chemistry* 2008, *33*(1), 99–105. doi:10.1007/s11243-007-9014-2.

[27] Halder, S.; Acharya, R.; Peng, S.-M.; Lee, G.-H.; Drew, M. G. B.; Bhattacharya, S. Synthesis, Structure, and Electrochemical Properties of a

Family of 2-(Arylazo)phenolate Complexes of Ruthenium with Unusual C−C Coupling and NN Cleavage. *Inorganic Chemistry* 2006, *45*(24), 9654–9663. doi:10.1021/ic060689u.

[28] Sarkar, A.; Pal, S. Complexes of oxomethoxovanadium(V) with tridentate thiobenzhydrazide based Schiff bases. *Inorganica Chimica Acta* 2008, *361*(8), 2296–2304. doi: 10.1016/j.ica.2007.10.053.

[29] Dash, S. P.; Pasayat, S.; Saswati; Dash, H. R.; Das, S.; Butcher, R. J.; et al. Oxovanadium(V) complexes incorporating tridentate aroylhydrazoneoximes: Synthesis, characterizations and antibacterial activity. *Polyhedron* 2012, *31*(1), 524–529. doi: 10.1016/j.poly.2011.10.017.

[30] Sobola, A.; Watkins, G. Antimicrobial activity and Cu(II) complexes of Schiff bases derived from ortho-aminophenol and salicylaldehyde derivatives. *Journal of Chemical and Pharmaceutical Research* 2013, *5*, 147–154.

[31] Karekal, M. R.; Biradar, V.; Bennikallu Hire Mathada, M. Synthesis, Characterization, Antimicrobial, DNA Cleavage, and Antioxidant Studies of Some Metal Complexes Derived from Schiff Base Containing Indole and Quinoline Moieties. *Bioinorganic Chemistry and Applications* 2013, *2013*, 1–16. doi:10.1155/2013/315972.

[32] Tadavi, S. K.; Yadav, A. A.; Bendre, R. S. Synthesis and characterization of a novel schiff base of 1,2-diaminopropane with substituted salicyaldehyde and its transition metal complexes: Single crystal structures and biological activities. *Journal of Molecular Structure* 2018, *1152*, 223–231. doi: 10.1016/j.molstruc.2017.09.112.

[33] Kuete, V.; Ngameni, B.; Tangmouo, J. G.; Bolla, J.-M.; Alibert-Franco, S.; Ngadjui, B. T.; et al. Efflux pumps are involved in the defense of Gram-negative bacteria against the natural products isobavachalcone and diospyrone. *Antimicrobial agents and chemotherapy* 2010, *54*(5), 1749–1752. doi:10.1128/AAC.01533-09.